The neutron dripline at Z = 4: the case of ^{13,15}Be

Anna Corsi, Belén Monteagudo, F. Miguel Marqués

To cite this version:

Anna Corsi, Belén Monteagudo, F. Miguel Marqués. The neutron dripline at Z = 4: the case of ^{13,15}Be. European Physical Journal A, 2021, 57 (3), pp.88. 10.1140/epja/s10050-021-00384-0 . hal-03171331

EPJ manuscript No.
(will be inserted by the editor)

The neutron dripline at Z=4: the case of ^{13,15}Be

Anna Corsi[1], Belen Monteagudo[2,3], and F. Miguel Marqués[2]

[1] CEA Saclay

[2] LPC Caen, Normandie Université, ENSICAEN, Université de Caen, CNRS/IN2P3, 14050 Caen, France

[3] NSCL

Received: date / Revised version: date

Abstract. We review an extensive study of the beryllium isotopic chain carried out at RIKEN. In particular, we discuss the results on ^{13,15}Be, two key isotopes for the understanding of dineutron configurations and decays in ^{14,16}Be. In the ^{13}Be case, a detailed analysis of its spectroscopy, including for the first time a well-founded reaction framework and a realistic three-body model of ^{14}Be that incorporates core excitations, confirms the dominant $\ell = 1$ content of the low-lying spectrum. In the ^{15}Be case, the fragmentation of ^{18}C, a priori free of any selection rules that may have precluded the observation of states in previous experiments, has confirmed the only known state at about 1.8 MeV, assigned according to shell-model calculations to a spin-parity $5/2^+$. Some perspectives of these studies are also given.

PACS. PACS-key discribing text of that key – PACS-key discribing text of that key

1 Introduction

The light neutron-rich nuclei have been a fertile ground for the study of exotic phenomena as halo and neutron clustering [1, 2]. Those arise from the combination of the shell evolution far from stability (disappearance of $N = 8, 20$ shell gaps) and the presence of weakly bound neutrons. The disappearance of the $N = 8$ gap was proposed already in 1960 [3] based on the observation of a $1/2^+$ (instead of $1/2^-$) spin-parity for the ground state for ^{11}Be [4]. Within the shell-model framework this can be interpreted as due to the lowering of the $1s_{1/2}$ single neutron orbital which becomes degenerated with the $0p_{1/2}$. Neutron knockout from the ground state of ^{12}Be suggests that only about 25% of the strength goes to the closed-shell configuration [5]. Furthermore, the lowering of the 2^+ and 1^- excited states

---

Send offprint requests to:

in ^{12}Be with respect to ^{11}Be, and the large B(E1; $0^+_{g.s.} \rightarrow 1^-$) [6, 7], confirm the strong configuration mixing between the *0p* and (*1s*,*0d*) shells due to the melting of the $N = 8$ gap.

^{11}Be was among the first nuclei for which halo existence was pinned down via reaction cross-section measurement [8] and observation of an enhancement close to the threshold of the E1 strength measured in Coulomb breakup [9]. The next halo nucleus in the Be chain is ^{14}Be [10], the heaviest bound isotope of the chain. It has the peculiarity of being a two-neutron halo and a Borromean nucleus, i.e. a three-body system (^{12}Be+$2n$) without any bound two-body subsystems. The correlation among the two halo neutrons appears as a key element to explain the stability of ^{14}Be. A first attempt to study the spatial configuration of those neutrons was a measurement of the correlation angle in one-neutron removal reactions [11]. An asymmetry in this distribution is interpreted as a signature of dineutron correlation. Such an asymmetry is observed in the case of ^{11}Li, for which strong indication of dineutron correlation already existed [12], while a weaker one is observed in the case of ^{14}Be.

Neutron-neutron correlations are a key element to understand the structure of ^{16}Be, too. The fact that ^{16}Be is expected to be bound with respect to neutron emission and unbound with respect to two-neutron emission, combined with the fact that ^{15}Be is expected to be unbound with respect to one neutron emission, make it a good candidate for a direct two-neutron decay to ^{14}Be. The possible decay patterns of ^{16}Be are determined by the availability of energetically accessible intermediate states in ^{15}Be. The ground state resonance of ^{15}Be has been measured at 1.54 MeV [13], above the ^{16}Be g.s., preventing a sequential decay through it. Furthermore, the two-body relative energy spectrum of the two neutrons measured in [14] suggests a dineutron emission directly to the ^{14}Be ground state.

Knowing the structure of the intermediate ^{13,15}Be unbound systems appears therefore as a key element to interpret the dineutron structure of ^{14,16}Be. Nevertheless, their energy spectrum is still not well established and the spin-parity assignment of the observed resonant structures is still tentative [13] or debated [15, 16, 17]. In this review, we will present recent results on the spectroscopy of ^{13,15}Be obtained at RIKEN using the SAMURAI spectrometer.

1.1 State of the art on ^{13}Be

^{13}Be is one-neutron unbound as suggested more than 50 years ago [18, 19], and confirmed in 1973 [20]. Several experiments have been performed to study the spectroscopy of ^{13}Be via missing mass and invariant mass techniques using charge exchange [21], fragmentation [22], proton removal from ^{14}B [23, 24, 17] and neutron removal from ^{14}Be [11, 15, 25, 16]. Resonances at ∼2, 5, 7, and 10 MeV [26], and at 1.22(10), 2.10(16), 4.14(12), 5.09(14), and 7.0(2) MeV [27] have been measured via the missing-mass method. Invariant mass spectra from different experiments display a peak at about 0.5 MeV above the ^{12}Be+n threshold, and a broad structure around 2 MeV. It is known that the spectral shape may strongly differ depending if ^{13}Be is produced starting from ^{14}Be [11, 15, 25, 16] or ^{14}B [23, 24, 17], but even using the same reaction mechanism different interpretations have been provided.

Ref. [15] interprets the low-lying peak as a $1/2^-$ ($\ell = 1$) intruder state that appears due to the quenching of the $N = 8$ spin-orbit shell gap, and the structure around 2 MeV as a $5/2^+$ ($\ell = 2$) state. This interpretation is based on the analysis of the transverse momentum distribution using s, p and d waves, corroborated by shell-model calculations, and is in agreement with predictions by [28]. Ref. [16] makes a synthesis of existing experimental results, with special emphasis on those reported in [11, 25, 15]. The analysis of the transverse momentum distribution performed in Ref. [16] via the momentum profile analysis technique (i.e. the variance of the transverse momentum distribution as a function of the relative energy) yields quite different conclusions with respect to Ref. [15]: a much stronger d-wave component (dominant above 2.6 MeV), and a dominance of s-wave (80(10)%) around 0.5 MeV, instead of p-wave (see Fig. 1).

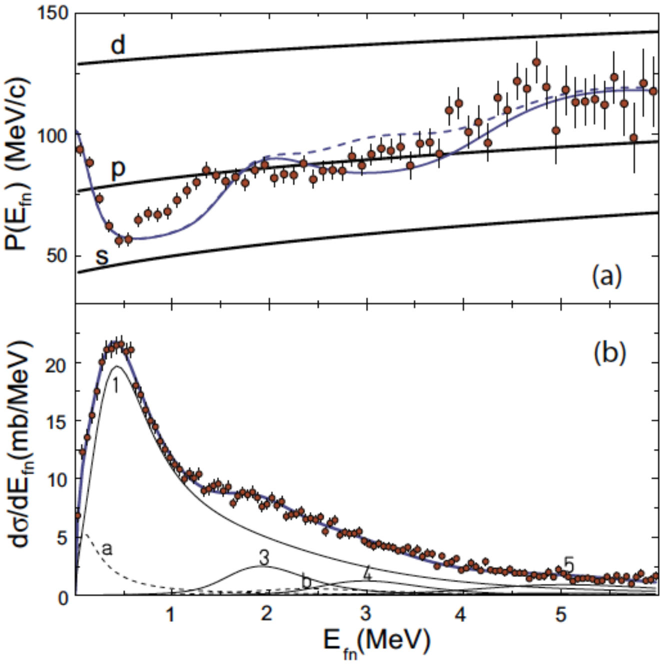

Fig. 1. Momentum profile (top) and ^{13}Be decay energy spectrum (bottom) consistently fitted with the superposition of resonant states, the main one (labeled 1) arising from the constructive interference of two $\ell = 0$ Breit-Wigner functions. Taken from [16].

This diversity and sometimes inconsistency in the interpretation of ^{13}Be relative-energy spectrum indicates that the standard fitting procedures used for the analysis of these spectra may be lacking some constraints when dealing with a complex spectrum composed of broad resonances.Part of the complexity of the ^{13}Be continuum spectrum stems from the admixtures of single-particle structures with core-excited components. In fact, core excitation has been postulated as a key element to understand the formation of Borromean systems [29, 30], but it is very difficult to pin down experimentally and to include in theoretical models for the structure of ^{14}Be.

1.2 State of the art on ^{15}Be

^{15}Be is also unbound with respect to one-neutron emission. Its complete level structure, although fundamental for the interpretation of the two-neutron decay of the neighbouring ^{16}Be, is still not well understood. Shell-model calculations [31] predict a $3/2^+$ ground state. The first excited state is expected to be a $5/2^+$ state, located just 300 keV above the ground state. Lying higher in energy, at roughly 1 MeV, a $1/2^+$ state is also predicted. Based on these predictions, the previous experiments have focused on determining which of the two low-lying states, either $3/2^+$ or $5/2^+$, is indeed the ground state of ^{15}Be. However, the systematics of the $N = 11$ isotones (ig. 1.2) show that all three levels might be instead closely spaced with, in fact, the $1/2^+$ being the ground state and $3/2^+$ lying just above $5/2^+$.

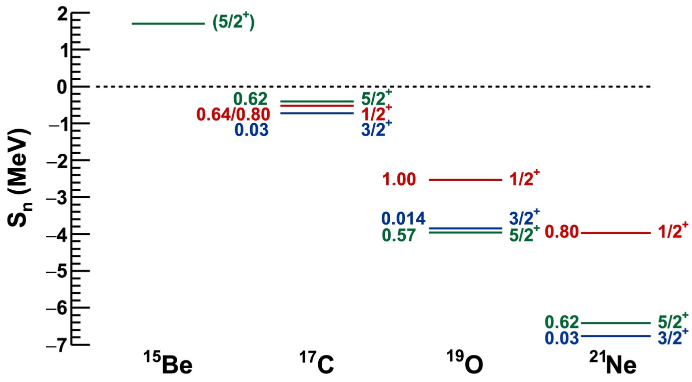

Fig. 2. Neutron binding energies of the positive parity states in the $N = 11$ isotonic chain and the corresponding experimental spectroscopic factors where available. Taken from [32].

Experimentally, only one state has been observed through a neutron transfer ^{14}Be$(d,p)^{15}$Be reaction [31]. The ^{14}Be+n decay energy spectrum from this experiment displays one resonance-like structure at 1.8(1) MeV that was identified with the $5/2^+$ excited state based on the decay patterns predicted by shell-model calculations. The $3/2^+$ state, predicted to be analogue to the ground state of the isotone ^{17}C, is expected to be very weakly populated via a neutron transfer. Instead, a direct two-proton knock-out reaction from a ^{17}C beam should have a high selectivity and strongly populate the $3/2^+$ state.

Two different experimental attempts have been reported to search for ^{15}Be using a two-proton removal reaction. No events in the ^{14}Be+n channel where observed in the first experiment [13] and thus a lower limit of 1.54 MeV above the threshold of neutron emission was established for the $3/2^+$. The large spectroscopic overlap with ^{12}Be(2^+), a state that decays via two-neutron emission to ^{12}Be$_{gs}$, motivated the study of the three neutron decay to ^{12}Be using as well a two-proton knockout reaction [33]. In this case, the analysis of the ^{12}Be+$3n$ spectrum concluded that no ^{15}Be component was needed to describe the experimental data. However, this study was inconclusive due to the low statistics that resulted from the application of the rejection of neutron cross-talk events. Therefore, the question about the energy and spin-parity of the ground state of ^{15}Be is still open.

1.3 Experimental setup at RIKEN

The experiments were performed at the Radioactive Isotope Beam Factory operated by the RIKEN Nishina Center and the Center for Nuclear Study (CNS) of the University of Tokyo. Secondary beams were produced and separated by the BigRIPS fragment separator [34], using projectile fragmentation of a ^{48}Ca primary beam at 345 MeV/nucleon on a Be target. Fragmentation products were detected and identified by using plastic scintillators and multi-wire drift chambers (MWDCs) positioned along the BigRIPS line. In this review we will show results from two SAMURAI experiments, the Day-One campaign in which ^{15,16}Be were searched for from several reaction channels, and the SAMURAI18 experiment in which ^{13,14,15,16}Be were measured in (p, pn) and $(p, 2p)$ reactions. For the details of the setups the reader can refer to Refs. [35, 36] and Ref. [37], respectively, below we will only highlight the basic elements.

During the Day-One campaign, a wide range of secondary beams were used, from the lightest ^{17}B up to the heaviest ^{28}Ne, with the main focus set on the study of the properties of ^{18,19}B, ^{21,22}C and ^{25,26}O, but with many additional reaction channels recorded in parallel. The different beams were accelerated at about 250 MeV/nucleon and impinged on a 1.8 g/cm^2 carbon target, surrounded by the NaI scintillators from the DALI2 array. The identification and momentum analysis of the heavy charged fragment was achieved via the combination of tracking in the SAMURAI dipole magnet [38] via a set of MWDC placed before and after the magnet (FDC1, FDC2), and the energy loss and time of flight measurement in an array of plastic scintillators placed at the focal plane of SAMURAI (HODF). Their momentum could then be deduced from the measurement of their trajectory. The dipole gap was kept under vacuum using a chamber equipped with thin exit windows [39] so as to reduce to a minimum the amount of material encountered by both the fragments and neutrons. The decay neutron was detected in the two walls of plastic scintillators of the NEBULA array [40]. A sketch of the SAMURAI setup is shown in Fig. 3, top.

During the SAMURAI18 experiment, a cocktail beam of ^{11}Li, ^{14}Be, and ^{17}B (80%, 12%, and 8%, respectively) at about 260 MeV/nucleon impinged on the hydrogen target of the MINOS device, conceived and built between 2011 and 2013 at the IRFU Institute of CEA Saclay with the support of a grant from the European Research Council.

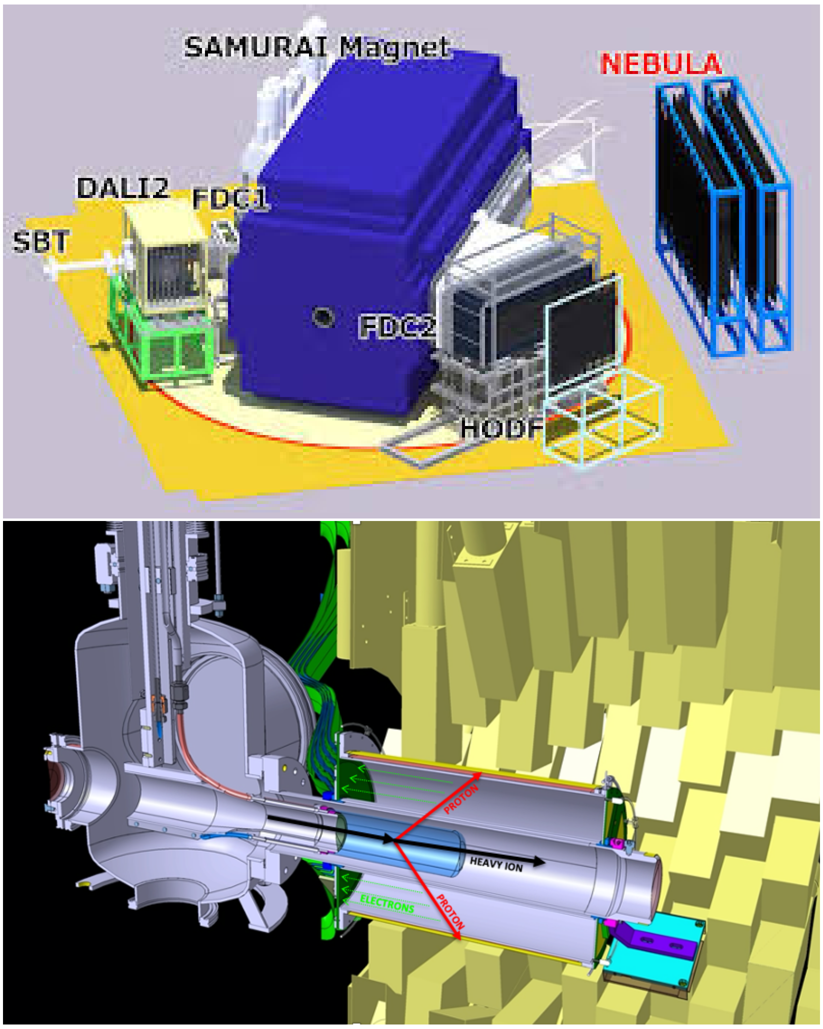

Fig. 3. Top: view of the SAMURAI setup. Bottom: the MINOS target (in blue) surrounded by the TPC (in grey) located inside the DALI2 array, with a $(p,2p)$ reaction displayed.

It consists of a liquid hydrogen target (LH_2) of cylindrical shape, available at different thicknesses (5, 10, 15 cm), surrounded by a Time Projection Chamber (TPC). In the TPC, electrons produced by the proton(s) traversing the gas of the chamber drift to a Micromegas detector (see Fig. 3, bottom) under the effect of a strong electric field. The drift time, combined with the pad position on the Micromegas plane, allows to reconstruct the proton track in 3D and, via intersection with the other proton (in the case of $(p,2p)$ reaction) or the heavy-ion trajectory (in the case of (p,pn) reaction), the reaction vertex. This information can be then used for Doppler correction (in the case of gamma spectroscopy) and for energy-loss correction (in the case of missing and invariant mass spectroscopy). In such a way one can increase the luminosity by using a thick target without degrading the resolution of the measurement. Fig. 3 shows the MINOS device surrounded by the gamma array DALI2.

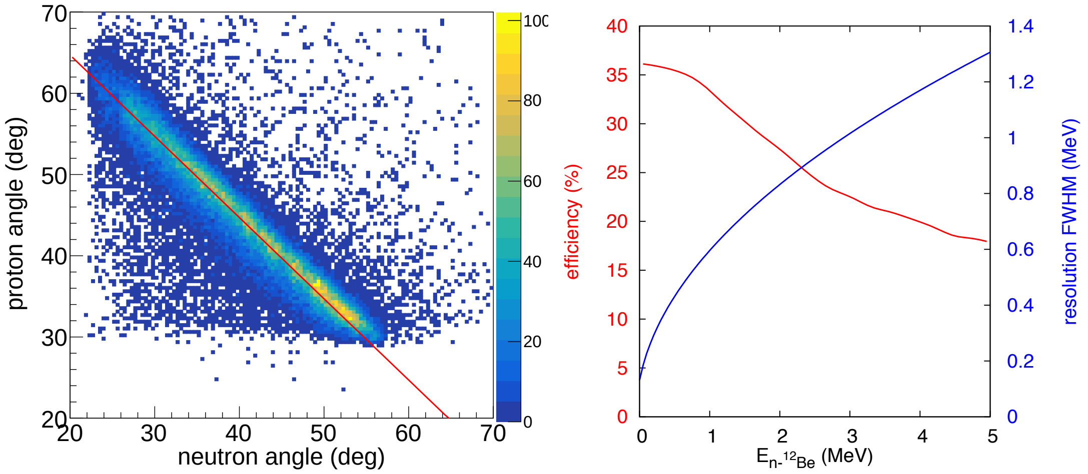

Fig. 4. Left: angular correlation in the laboratory frame of proton and neutron in the ^{14}Be(p, pn) reaction. The red line corresponds to the kinematics calculated with the QFS code of Ref. [41]. Right: typical efficiency (red line) and resolution (blue line) for ^{13}Be invariant mass measurement with NEBULA and SAMURAI. Taken from [37].

The MINOS device was surrounded by a reduced version of DALI2 in order to avoid interference with the (p, pn) measurement. Two additional detectors were set up around the target area in order to measure respectively the proton and the neutron issued from the (p, pn) reaction. For the events including the detection of a neutron and a proton, we could check that the kinematic conditions corresponding to Quasi-Free scattering (QFS) were respected. QFS is a proton-induced one-nucleon removal reaction, where the probe selectively removes one nucleon leaving the remaining nucleus intact. The opening angle between the two should approach 90°, i.e. the opening angle for elastic scattering. Due to the fact that the scattered neutron is bound, this angle is slightly smaller. In the case of ^{14}Be(p, pn) it is expected to be 86°, in very good agreement with the data (Fig. 4, left). Due to our strong triggering condition, when requiring the detection of one proton at angles between 30° and 70°, QFS events dominate the collected statistics.

The efficiency of the NEBULA array for the detection of one neutron is $\sim 35\%$ at these beam energies. Invariant-mass resolution and efficiency as a function of the relative energy of the decay have been determined via a GEANT4 simulation [42] with the code used in [40]. The resolution follows a FWHM=$0.587\sqrt{E_r}$ MeV law and is shown in Fig. 4, right, together with the efficiency.

2 Spectroscopy of ^{13}Be

As discussed in the introduction, the inconsistency of the different interpretations of ^{13}Be experiments requires a step forward in the quality of the data and the sensitivity of the probe, but also in the constraints from the theory. In the following we will discuss both aspects.

2.1 Results from SAMURAI18

The main asset of this new measurement of the spectroscopy of ^{13}Be is the capability to select QFS process and measure with high statistics ^{12}Be-n-γ coincidences. The invariant-mass spectrum of ^{13}Be is shown in Fig. 5, left. The spectrum is characterized by a peak with maximum at ~ 0.48 MeV and a broader structure, peaked at ~ 2.3 MeV, extending from $\sim$ 1–5 MeV. The absolute cross section is determined taking into account the efficiency for invariant-mass measurement and the fragment transmission. The error bars take into account the uncertainty on the transmission (1%), on the neutron detection efficiency (2.5%) and the statistical uncertainty on the number of beam and fragment particles.

The γ-ray spectrum of ^{12}Be is shown in Fig. 5, right. The 2.1(0.1) and 2.7(0.4) MeV transitions are consistent with the known transitions deexciting the 2^+ and 1^- excited states of ^{12}Be to its ground state. We note that the same gamma transitions were observed in Ref. [15], though with very limited statistics, while Ref. [17] observed only the 2.1 MeV transition. The contribution corresponding to the decay through ^{12}Be(2^+) and ^{12}Be(1^-) excited states has been determined via coincidences with 2.1 and 2.7 MeV gamma transitions, respectively, and is shown for comparison after correcting for gamma-detection efficiency. The 6% uncertainty on gamma detection efficiency has been added to the error bars. As can be better seen in the inset of Fig. 5, left, the 2.1 MeV transition is observed in coincidence with a structure peaking at ~ 0 and ~ 3 MeV in the relative energy spectrum, as in Ref. [17]. The 2.7 MeV one is observed in coincidence with a structure at ~ 3 MeV only. The contribution from the Compton events associated to the 2.7 MeV transition summing up to the 2.1 MeV transition has been estimated via the simulation and subtracted from the cross section.

Based on this, we built a partial level scheme presented in Fig. 6. The 2.3 MeV peak observed in the relative energy spectrum likely corresponds to the well-accepted $5/2^+$ state in ^{13}Be, whose tail may be responsible for the ~ 0 MeV transition in coincidence with the 2^+ state in ^{12}Be (see Ref. [16]). The spin-parity assignment of the levels shown in Fig. 5 will be further discussed in Sec. 2.2, where we also analyze the information from the corresponding transverse momentum distributions.

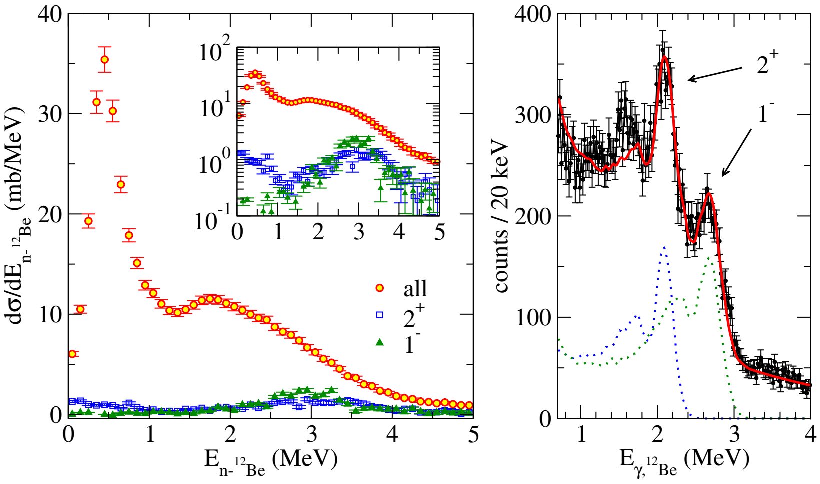

Fig. 5. Left: relative energy spectrum of ^{13}Be and contributions from core excited components. The inset shows the spectrum in logarithmic scale. Right: gamma spectrum of ^{12}Be. The two transitions are reproduced by the sum of an exponential background and the response functions (dashed curves) of DALI2 to a transition at 2.1 MeV and 2.7 MeV, obtained via a GEANT4 simulation. Taken from [37].

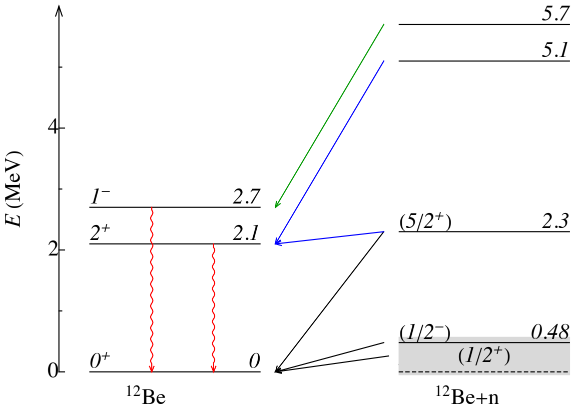

Fig. 6. Partial level scheme based on the observed neutron-^{12}Be relative energy spectrum and gamma-neutron-^{12}Be coincidences. Transitions in the relative energy spectrum are represented by lines (black for transitions to the ground state of ^{12}Be, blue and green for transitions populating ^{12}Be(2$^+$) and ^{12}Be(1$^-$), respectively). Gamma transitions are represented by the red wavy arrows. Energies are given in MeV. Taken from [37].

2.2 Theoretical analysis

The structure of ^{13}Be is a key input in the three-body models of ^{14}Be. On the other hand, the structure of ^{14}Be, and the specific (p, pn) reaction used, will also dictate the states that we will populate in ^{13}Be. We will therefore discuss the three-body calculations and the reaction model.

2.2.1 Three-body calculations

In order to better understand the experimental results, we have performed structure calculations for ^{14}Be using a three-body model (^{12}Be$+n+n$) within the hyperspherical formalism [43, 44, 45]. Details on the formalism can be found, for instance, in Ref. [46] and references therein. Three-body calculations require, as input, the binary interactions between all constituents. For the n-n potential, we employ the GPT tensor interaction [47] which reproduces NN observables up to 300 MeV. In order to get a realistic description of ^{14}Be, the ^{12}Be-n interaction needs to reproduce the properties of the unbound subsystem ^{13}Be. Since there is no consensus on the interpretation of the ^{13}Be spectrum, we tried different core-neutron potentials to study the sensitivity of the structure and reaction observables to the properties of ^{13}Be.

In order to include some excited-core components in the description of ^{14}Be, we parametrize the ^{12}Be-n interaction as a deformed Woods-Saxon potential with ℓ-dependent central and spin-orbit terms. Following Ref. [48], we introduce an effective quadrupole deformation parameter of $\beta_2 = 0.8$, and the 0^+ ground state and the first 2^+ excited state in ^{12}Be are coupled by means of a simple rotational model [44]. In this scheme, no other excited states of ^{12}Be are included. As shown in Ref. [48], despite the deformation the s-wave interaction still gives rise to a $1/2^+$ virtual state in ^{13}Be. The potential parameters $V_c^{(0,2)}$ and V_{ls} are adjusted to fix the scattering length of this virtual state and to provide a $5/2^+$ resonance just below the 2^+ excitation threshold in ^{12}Be, i.e. at 2.11 MeV [49]. Note that, in this scheme, the $5/2^+$ state may decay via $d_{5/2}$ neutrons to the ground state of ^{12}Be, but also via $s_{1/2}$ to the 2^+ excited state, given its finite width. For simplicity, we started with a potential P1 without negative-parity resonances but given the open debate about the presence of a low-lying p-wave resonance in ^{13}Be, we considered an additional potential P2 including a p-wave. The resulting ^{14}Be properties are also shown in Table 1.

	a	$E(5/2^+)$	$\Gamma(5/2^+)$	$E(1/2^-)$	$\Gamma(1/2^-)$	s	p	d	2^+
P1	-40.1	1.96	0.27	-	-	0.59	0.13	0.26	0.34
P2	-9.2	1.96	0.27	0.46	0.40	0.19	0.62	0.18	0.22

Table 1. Scattering length a (in fm) of the $1/2^+$ virtual state in ^{13}Be and energies and widths of the $5/2^+$ and $1/2^-$ resonances (in MeV) using the different core-neutron potentials P1 and P2. On the right, the resulting properties of the ^{14}Be ground state: partial wave content for $L = 0, 1, 2$ neutrons, and weight of the 2^+ core-excited components.

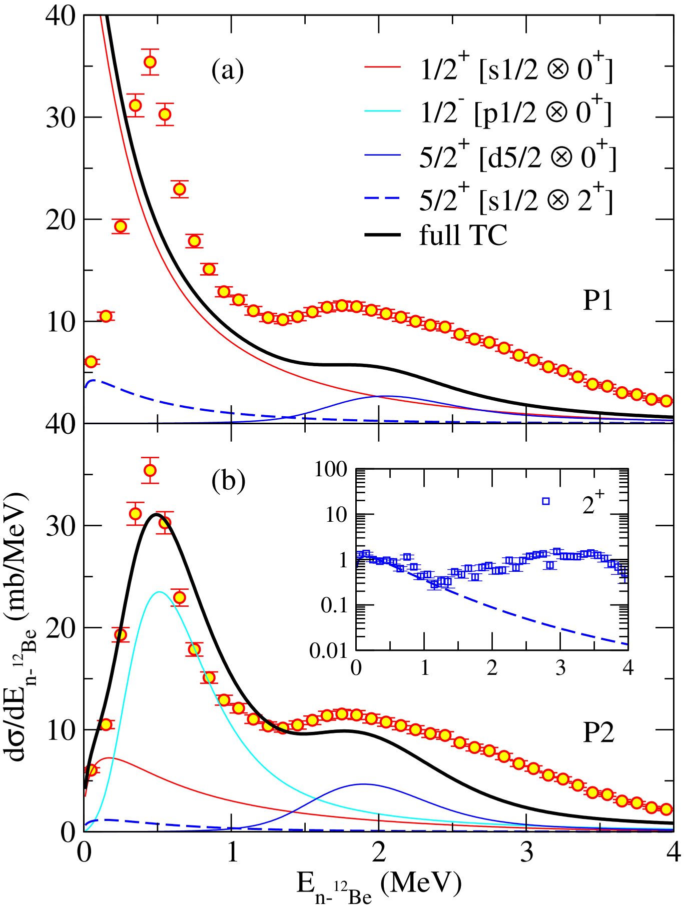

Fig. 7. ^{13}Be relative-energy spectrum using the (a) P1 and (b) P2 potentials [37]. Results are shown after convoluting the theoretical lineshapes with the experimental resolution function. The inset shows the relative energy spectrum measured in coincidence with the ^{12}Be(2^+) decay transition, compared to the calculated core-excited component. See text for details.

2.2.2 Reaction calculations

To discriminate among those inputs for ^{14}Be, we have compared the present (p,pn) data with reaction calculations based on the so-called Transfer to the Continuum (TC) framework [50]. Within TC, the differential cross-section for the (p,pn) reaction is obtained from the prior-form transition amplitude leading to the three-body continuum states for $p+n+{}^{13}$Be. TC was recently extended to describe processes induced by Borromean projectiles [51].

The model considers a spectator/participant scenario, in which the incident proton is assumed to remove one of the valence neutrons without modifying the state of the remaining ^{13}Be (^{12}Be$\,+\,n$) subsystem. This is consistent with QFS conditions. Under this assumption, the ^{14}Be structure enters through the overlap functions between the initial state (the ^{14}Be g.s.) and the final ^{13}Be states so that the cross-section for different configurations of ^{13}Be (defined by their energy $E_{n-^{12}\mathrm{Be}}$ and angular momentum and parity J^{π}_{T}) can be computed independently.

Important ingredients are also the proton-neutron and nucleon-^{13,14}Be interactions. For the former, following previous applications of the method [50, 51], we adopt the Reid93 parametrization [52], which provides an accurate description of the proton-neutron cross sections and phase-shifts up to 350 MeV. For proton-^{14}Be and proton/neutron-^{13}Be interactions, which take into account the distortion and absorption of the incoming proton and of the outgoing nucleons, we employ the optical potentials computed from the Dirac phenomenological parametrization [53, 54].

The $^{12}\mathrm{Be} + n$ relative-energy spectrum obtained by using the P1 core-neutron potential and convoluting with the experimental resolution from the simulation (determined as explained in Sec. 2) is shown in Fig. 7a. Note that these reaction calculations provide absolute cross-sections, so no fitting or scaling is carried out. The different contributions are labeled $J_T[L_J \otimes I]$, where J_T is the total ^{13}Be angular momentum resulting from coupling the single-particle configuration L_J with the spin I of ^{12}Be. Trivially, since the spin of ^{14}Be is 0^+, J_T equals $j_2 = [l_2 \otimes s_2]$, the angular momentum of the removed nucleon.

The cross-section using P1 overestimates the experimental data at low relative energies, due to the large scattering length of the s-wave virtual state, and does not reproduce the maximum around 0.5 MeV. A much better agreement is found using potential P2, as shown in Fig. 7b. Variations of P2 have been attempted but finally P2 itself appeared to be the best choice. This is a clear indication that a low-lying resonance is required to describe the ^{13}Be spectrum. The theoretical distribution is somewhat broader than the experimental data, and it underestimates them at large relative energies. Overall, this suggests that p-wave content obtained with the P2 potential is perhaps too large and that there might be missing components in the wave-function expansion, in particular those coming from the coupling to other excited states of ^{12}Be. Calculations including these features are not yet available.

The ^{13}Be data can be further studied using the transverse momentum distributions of the knocked-out neutron. The comparison between the present calculations, using potential P2, and the experimental momentum distributions is presented in Fig. 8, for three different relative-energy bins: 0–0.2, 0.4–0.5 and 1.8–2.2 MeV. Calculations have been convoluted with the experimental resolution on fragment momentum of $\sim$ 39 MeV/c (FWHM) obtained from the direct beam measurement. The overall normalization of the total theoretical distribution with respect to the data has been adjusted to obtain the best χ^2 fit. Individual contributions from the different orbital angular momenta of the knocked-out neutron are also presented. The relative weights of these contributions are fixed by the structure and reaction calculations.

Overall, it is found that the width of the momentum distributions is well reproduced. In particular, we can describe the data at 0.4–0.5 MeV with a dominant p-wave contribution. In Ref. [16], an s-wave resonance (or a combination of two overlapping s-wave resonances) was proposed to explain the peak in the ^{13}Be spectrum.

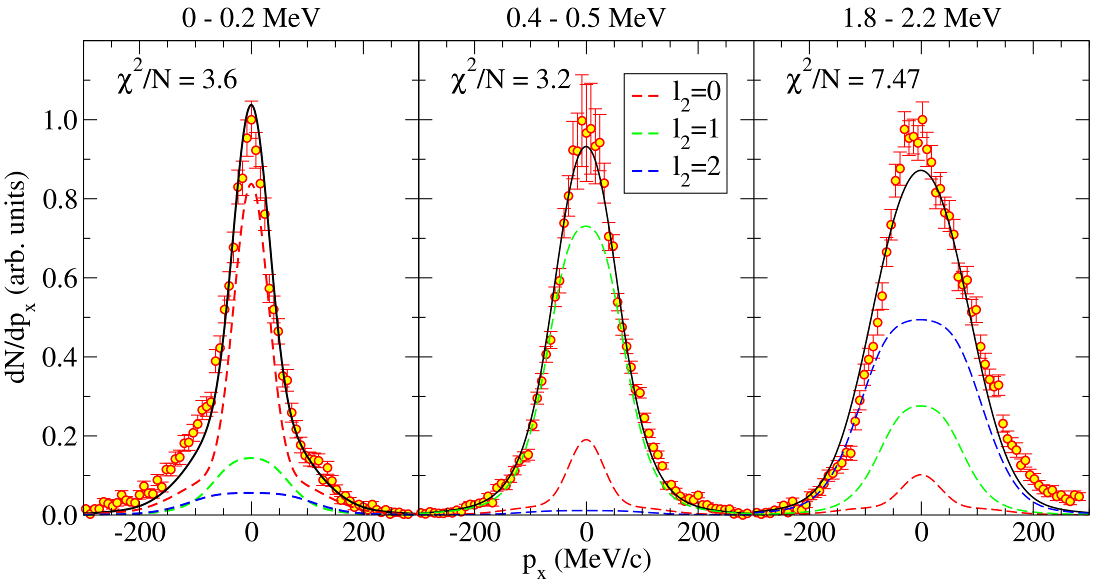

Fig. 8. Experimental transverse momentum distributions in the 0-0.2, 0.4-0.5 and 1.8-2.2 MeV relative energy range [37]. The solid black line is the total TC result, convoluted with the experimental resolution and rescaled through a χ^2 fit. Dashed lines are the contributions corresponding to removal of a neutron from a *s*- (red), *p*- (blue) or *d*-wave (green).

2.3 Conclusions

The main conclusion of our analysis of ^{13}Be spectroscopy is the assignment of a dominant $\ell = 1$ contribution of the resonant peak observed in the low-lying spectrum, in agreement with [15, 17] and at variance with the conclusions of Refs. [25, 16], which assigned a dominant $\ell = 0$ nature to this peak. The novelty of our method consists in calculating, for the first time, the relative energy cross-section and momentum distribution using a well-founded reaction framework and a realistic three-body model of ^{14}Be that incorporates ^{12}Be(2^+) excitations, instead of extracting individual angular momentum components from a fit, a technique that becomes more ambiguous in the case of complex spectra as the one of ^{13}Be. More details on this analysis have been published in [37].

3 Spectroscopy of 15Be

As mentioned in the introduction, ^{17}B was one of the beam particles accelerated in SAMURAI18, with the aim to probe states in both ^{15,16}Be. During the Day-One campaign, ^{17}B was the lightest beam used, but other neighbouring particles were also accelerated (like ^{19}B or $^{18-20}$C). Since ^{17}C (the isotone of ^{15}Be) was not part of the beam particles available, ^{15}Be was populated in both experiments through fragmentation reactions.

3.1 Results from SAMURAI18

The ^{17}B$(p, 2p)$ reaction populated two clear structures in the ^{14}Be+$2n$ relative-energy spectrum, that were associated with the ground (0^+) and first excited (2^+) states of ^{16}Be, at respectively 0.84 and 2.15 MeV [55, 56]. Three-body calculations with a model similar to the one described for the ^{14}Be analysis are in progress, and a publication of the thorough analysis of these results is in preparation. Concerning ^{15}Be, the main result of this experiment is that no states have been populated, since the states in ^{16}Be seem to decay directly to ^{14}Be [56].

3.2 Results from Day-One Campaign

The question of which of the predicted low-lying states, $5/2^+$, $3/2^+$ and $1/2^+$, corresponds to the ground state of ^{15}Be is still unanswered. Neither a two-proton removal reaction nor a neutron transfer have been successful due largely to the high selectivity dominating the reactions and the decay patterns. Heavier beams than ^{17}C can potentially populate states in ^{15}Be which would be inaccessible due to the selection rules that govern the direct knock-out reaction from ^{17}C. These fragmentation reactions would follow the removal of several nucleons in a single or multi-step process, the latter involving the population of an intermediate isotope that would decay into ^{15}Be.

During the Day-One campaign the ^{14}Be+n exit channel has been populated with a variety of beams, in particular ^{17,19}B, $^{18-20}$C and ^{22}N. Concerning the ^{17}B data, although the statistics and resolution are lower than in the SAMURAI18 data set due to the use of a carbon target instead of MINOS, the results are consistent. Two states were populated in ^{16}Be, and none in ^{15}Be [56]. In search of a reaction channel that did populate resonances in ^{15}Be we have considered the ^{18}C beam, and will describe the results in the following.

The relative-energy spectrum was reconstructed using the invariant-mass technique from the momenta of the coincident ^{14}Be+n events, with the selection of the fastest neutron arriving to the NEBULA detector. As shown in Fig. 9, there are two main structures that can be differentiated, one at around ~ 0.5 MeV, followed by a broader one that goes from 1.5–2.5 MeV. These structures, however, do not necessarily involve the direct population of resonances in ^{15}Be, as a fragmentation reaction from ^{18}C can potentially populate other isotopes that would equally contribute to the ^{14}Be+n decay spectrum.

One of the main non-resonant contributions to the relative energy spectrum may come from the population and decay of the heavier beryllium isotope, ^{16}Be. This isotope is unbound with respect to two-neutron emission and will decay into ^{14}Be$+n+n$. The triple events in the ^{18}C channel, despite the limited statistics, show a prominent peak associated with the ground state of ^{16}Be [56]. According to the SAMURAI18 results, the ground state decays directly

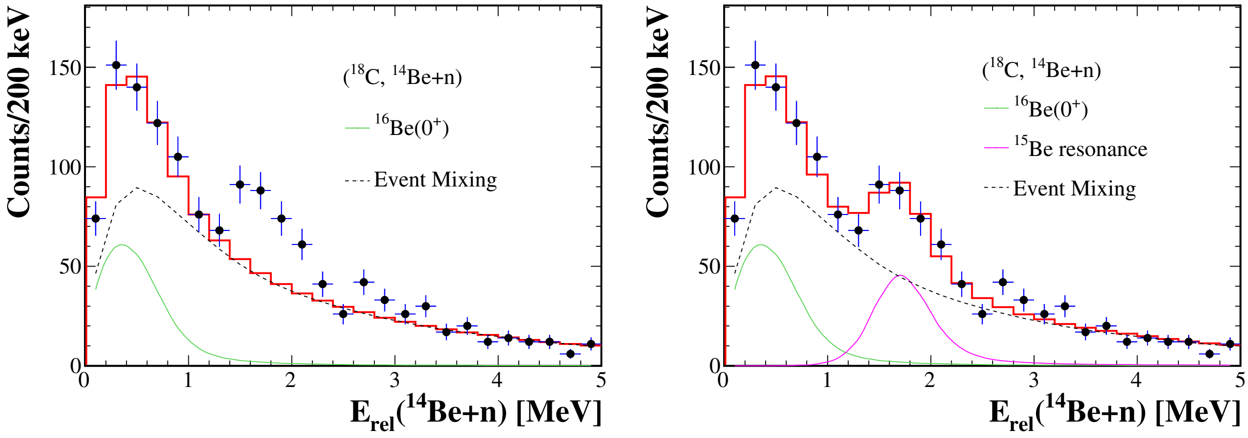

Fig. 9. ^{14}Be+n relative-energy spectrum following a fragmentation reaction from a ^{18}C beam at 242 MeV/nucleon. On the left, the non-resonant contributions that do not imply the population of states in ^{15}Be have been maximized: the fragment-n non-resonant contribution (dotted black line) calculated using the event-mixing technique, and the decay of ^{16}Be ground state (green line). A fit considering a ^{15}Be state at E=1.8 MeV is shown on the right.

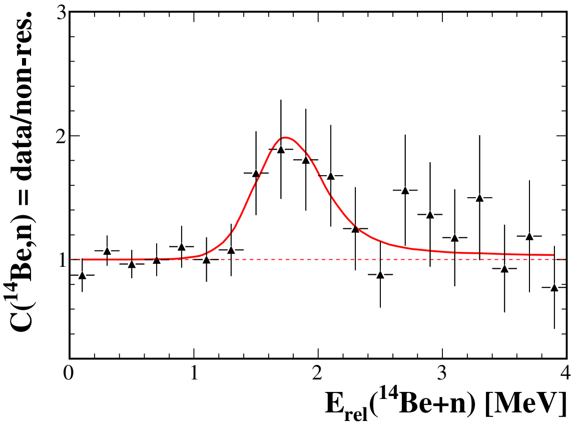

Fig. 10. Correlation function for ^{15}Be. The data points correspond to the experimental spectrum divided by the contributions that do not involve resonances in ^{15}Be (the red histogram in Fig. 9, left). The red line corresponds to the ratio of the two red histograms in Fig. 9, the one containing a ^{15}Be resonance and the non-resonant one.

towards ^{14}Be and no signature for sequential decay is observed. Therefore, ^{14}Be+n events coming from the decay of ^{16}Be will follow the corresponding phase space of that decay.

Another important non-resonant source comes from the direct population of ^{14}Be ground state. In that case, no ^{15}Be or ^{16}Be are populated and a coincident neutron with a ^{14}Be is a non-correlated event, being the neutron the product of unrelated intermediate steps. A non-correlated continuum can be calculated using the technique of event-mixing. This technique estimates the non-correlated contribution to the spectrum using the experimental data itself, by mixing a neutron and a ^{14}Be fragment from different events to create virtual pairs. The non-correlated distribution that results from these virtual pairs includes the experimental acceptances and responses as it is built from the actual detected particles. The reader can refer to Refs. [24, 36] for more details on the procedure.

At a first stage, the contribution of the two non-resonant components (the direct population of ^{14,16}Be) to the relative-energy spectrum has been maximized, without considering any ^{15}Be resonances. The left of Fig. 9 shows the description of the experimental spectrum using the maximized non-resonant components. The relative weight of the fragment-n non-correlated distribution (dotted black line) and the decay of ^{16}Be(0^+) (green line) is the free parameter in this first attempt to describe the ^{14}Be+n spectrum. It is clearly seen that the non-resonant contributions cannot be responsible for the structure at 2 MeV.

We define the correlation function C(^{14}Be,n) as the ratio between the experimental data and the maximized non-resonant contribution not related to the population of ^{15}Be (the red histogram in Fig. 9, left). The C(^{14}Be,n) distribution will be flat and equal to 1 if no ^{15}Be resonances are needed to describe the data. On the contrary, deviations from a flat distribution will reveal structures in the spectrum that are potentially resonances in ^{15}Be. Fig. 10 shows the application of the correlation function to our set of data. A clear peak-like structure at about ~ 2 MeV indicates the population of at least one resonance in ^{15}Be.

A fit to the relative-energy spectrum has been performed allowing for a resonance in ^{15}Be, in addition to the fragment-n component and the decay from ^{16}Be. The free parameters of the fit are the E and Γ of the ^{15}Be state as well as the relative weight of the three considered components. The right of Fig. 9 shows the best fit to the data. A ^{15}Be resonance of energy $E = 1.70 \pm 0.13$ MeV and width $\Gamma > 200$ keV (pink line) was found to describe the decay energy spectrum. Since the fit was not very sensitive to the value of Γ, only a lower limit can be given for this parameter. The red line in Fig. 10 corresponds to the ratio between the two red histograms in Fig. 9, in very good agreement with the experimental correlation function.

3.3 Conclusions

This result confirms the only state observed in ^{15}Be up to date [31], measured at the same energy and assigned to a spin-parity of $5/2^+$. If this is the case, the predicted $1/2^+$ and $3/2^+$ states would remain unobserved, as it seems also from the preliminary analysis of the other Day-One reaction channels [56]. It could be that the unobserved states are completely degenerate with the $5/2^+$, or that they decay exclusively to ^{12}Be+3n and would thus be absent from the ^{14}Be+n channel.

4 Summary and perspectives

We have reviewed the results from two SAMURAI campaigns, Day-One and SAMURAI18, in which an extensive study of the beryllium isotopic chain has been carried out. The knowledge on the structure of ^{13,15}Be, important for the understanding of dineutron configurations and decays in ^{14,16}Be, has been improved. In the ^{13}Be case, a qualitative step forward has been taken, using for the first time a well-founded reaction framework and a realistic three-body model of ^{14}Be that incorporates core excitations. These tools have allowed an unambiguous confirmation of the dominant $\ell = 1$ content of the low-lying spectrum. In the ^{15}Be case, the fragmentation of ^{18}C, *a priori* free of any selection rules that may have precluded the observation of states in previous experiments, has confirmed the only known state at about 1.8 MeV, assigned to a spin-parity $5/2^+$. Other predicted states remain thus unobserved.

The qualitative improvement has been made possible in part thanks to the MINOS device, a thick liquid hydrogen target with tracking capabilities. Interesting perspectives are being opened with a new such device, STRASSE, under construction at Darmstadt Technical University, that pushes the MINOS concept to even higher vertex tracking resolution. With these new capabilities, and the extension of the NEBULA neutron detector at SAMURAI, even heavier isotopes of beryllium may be accessible soon. Proposals to measure for the first time ^{17,18}Be are in preparation, that will open the field of neutron correlations in beryllium to the $3n$ and $4n$ cases. If the $N = 14$ shell closure provides extra binding to ^{18}Be with respect to ^{16}Be, ^{18}Be would become a candidate for direct $4n$ decay.

5 Acknowledgements

This work has been supported by the European Research Council through the ERC Starting Grant No. MINOS-258567. F.M.M. acknowledges partial support from the Franco-Japanese LIA-International Associated Laboratory for Nuclear Structure Problems as well as the French ANR14-CE33-0022-02 EXPAND.

References

1. I. Tanihata et al. *Phys. Rev. Lett.*, 55:2676–2679, Dec 1985.
2. K. Kisamori et al. *Phys. Rev. Lett.*, 116:052501, Feb 2016.
3. I. Talmi and I. Unna. *Phys. Rev. Lett.*, 4:469–470, May 1960.
4. D. H. Wilkinson and D. E. Alburger. *Phys. Rev.*, 113:563–571, Jan 1959.

5. A. Navin et al. *Phys. Rev. Lett.*, 85:266, Jul 2000.
6. H Iwasaki et al. *Physics Letters B*, 481(1):7 – 13, 2000.
7. H. Iwasaki et al. *Physics Letters B*, 491(1):8 – 14, 2000.
8. M. Fukuda et al. *Physics Letters B*, 268(3):339 – 344, 1991.
9. N. Fukuda et al. *Phys. Rev. C*, 70:054606, Nov 2004.
10. M. Labiche et al. *Phys. Rev. Lett.*, 86:600–603, Jan 2001.
11. H. Simon et al. *Nucl. Phys. A*, 791:267, 2007.
12. T. Nakamura et al. *Phys. Rev. Lett.*, 96:252502, Jun 2006.
13. A. Spyrou et al. *Phys. Rev. C*, 84:044309, Oct 2011.
14. A. Spyrou et al. *Phys. Rev. Lett.*, 108:102501, Mar 2012.
15. Y. Kondo et al. *Phys. Lett. B*, 690:245, 2010.
16. Y. Aksyutina et al. *Phys. Rev. C*, 87:064316, Jun 2013.
17. G. Ribeiro et al. *Phys. Rev. C*, 98:024603, Aug 2018.
18. A. M. Poskanzer, S. W. Cosper, Earl K. Hyde, and Joseph Cerny. *Phys. Rev. Lett.*, 17:1271, Dec 1966.
19. A. G. Artukh et al. *Phys. Lett. B*, 33:407, 1970.
20. J. D. Bowman, A. M. Poskanzer, R. G. Korteling, and G. W. Butler. *Phys. Rev. Lett.*, 31:614, Aug 1973.
21. B. R. Marks et al. *Phys. Rev. C*, 92:054320, Nov 2015.
22. M. Thoennessen, S. Yokoyama, and P. G. Hansen. *Phys. Rev. C*, 63:014308, Dec 2000.
23. J. L. Lecouey. *Few-Body Systems*, 34:21, May 2004.
24. G. Randisi et al. *Phys. Rev. C*, 89:034320, Mar 2014.
25. Yu. Aksyutina et al. *Phys. Lett. B*, 718:1309, 2013.
26. A.A. Korsheninnikov et al. *Phys. Lett. B*, 343:53, 1995.
27. A.V. Belozyorov et al. *Nucl. Phys. A*, 636:419, 1998.
28. G. Blanchon, A. Bonaccorso, D.M. Brink, A. García-Camacho, and N. Vinh Mau. *Nucl. Phys. A*, 784:49, 2007.
29. I. Tanihata et al. *Phys. Rev. Lett.*, 100:1, 2008.
30. G. Potel, F. Barranco, E. Vigezzi, and R. A. Broglia. *Phys. Rev. Lett.*, 105:9, 2010.
31. J. Snyder et al. *Phys. Rev. C*, 88:031303, Sep 2013.
32. X. Pereira-Lopez et al. *Physics Letters B*, 811:135939, 2020.
33. A. N. Kuchera and otehrs. *Physical Review C*, 91, 2015.

34. N. Fukuda, T. Kubo, T. Ohnishi, N. Inabe, H. Takeda, D. Kameda, and H. Suzuki. *Nucl. Instr. Meth. B*, 317:323 – 332, 2013.
35. Y. Kondo et al. *Phys. Rev. Lett.*, 116:102503, Mar 2016.
36. S. Leblond et al. *Phys. Rev. Lett.*, 121:262502, Dec 2018.
37. A.Corsi et al. *Phys. Lett. B*, 797:134843, 2019.
38. T. Kobayashi et al. *Nucl. Instrum. Methods Phys. Res. B*, 317:294, 2013.
39. Y. Shimizu et al. *Nucl. Instr. Meth. B*, 317:739, 2013.
40. T. Nakamura and Y. Kondo. *Nucl. Instrum. Methods Phys. Res. B*, 376:156, 2016.
41. V. Panin et al. *Phys. Lett. B*, 753:204, 2016.
42. S. Agostinelli et al. *Nucl. Instr. Meth. A*, 506(3):250, 2003.
43. P. Descouvemont, C. Daniel, and D. Baye. *Phys. Rev. C*, 67:044309, Apr 2003.
44. I.J. Thompson, F.M. Nunes, and B.V. Danilin. *Comput. Phys. Commun.*, 161:87, 2004.
45. M. Rodríguez-Gallardo, J. M. Arias, J. Gómez-Camacho, A. M. Moro, I. J. Thompson, and J. A. Tostevin. *Phys. Rev. C*, 72:024007, Aug 2005.
46. J. Casal, E. Garrido, R. de Diego, J. M. Arias, and M. Rodríguez-Gallardo. *Phys. Rev. C*, 94:054622, Nov 2016.
47. D. Gogny, P. Pires, and R. De Tourreil. *Phys. Lett. B*, 32:591, 1970.
48. T. Tarutina, I.J. Thompson, and J.A. Tostevin. *Nucl. Phys. A*, 733:53, 2004.
49. J. H. Kelley, J. E. Purcell, and C. G. Sheu. *Nucl. Phys. A*, 968:71, 2017.
50. A. M. Moro. *Phys. Rev. C*, 92:044605, Oct 2015.
51. M. Gómez-Ramos, J. Casal, and A. M. Moro. *Phys. Lett. B*, 772:115, 2017.
52. V. G. J. Stoks, R. A. M. Klomp, C. P. F. Terheggen, and J. J. de Swart. *Phys. Rev. C*, 49:2950, Jun 1994.
53. S. Hama, B. C. Clark, E. D. Cooper, H. S. Sherif, and R. L. Mercer. *Phys. Rev. C*, 41:2737, Jun 1990.
54. E. D. Cooper, S. Hama, B. C. Clark, and R. L. Mercer. *Phys. Rev. C*, 47:297, Jan 1993.
55. B. Monteagudo et al. In *Recent Progress in Few-Body Physics*, pages 331–335, Cham, 2020. Springer International Publishing.
56. Belen Monteagudo Godoy. *Structure and neutron decay of the unbound Beryllium isotopes 15,16Be.* Theses, Normandie Université, November 2019.